Molecular Catalysis 553 (2024) 113736

Contents lists available at ScienceDirect

Molecular Catalysis

journal homepage: www.journals.elsevier.com/molecular-catalysis

Copper nanoparticles embedded into nitrogen-doped carbon fiber felt as recyclable catalyst for benzene oxidation under mild conditions

Somayeh Tavasolikejani [a], Sayyed Mahdi Hosseini [a,*], Mehran Ghiaci [a], Thomas Vangijzegem [b], Sophie Laurent [b]

[a] Department of Chemistry, Isfahan University of Technology, Isfahan 8415683111, Iran
[b] NMR and Molecular Imaging Lab, General, Organic and Biomedical Chemistry Unit, University of Mons, Mons B-7000, Belgium

ARTICLE INFO

Keywords:
Copper nanoparticles
Carbon fiber felts
Oxidation
Benzene
Phenol
Nanocatalyst

ABSTRACT

Herein, an active and stable nanocatalyst based on copper nanoparticles embedded into nitrogen-doped carbon fiber felts (N—CFFs) was fabricated through a co-assembly protocol. The catalytic performance of Cu (20 wt. %)/N—CFF was contributed to its structural and morphological features, which were studied by various characterization techniques. The data illustrated that the catalyst showed reasonable activity and excellent selectivity in oxidation of benzene-to-phenol (25.2 and 100% for yield and selectivity respectively) in the presence of an environmentally-friendly oxidant. Furthermore, the microscopic catalyst kept its long-term performance until nine successive runs, which turns it into a bulk alternative in large-scale schemes.

1. Introduction

Carbon Fiber Felts (CFFs) refers to a type of monolithic supports containing straight channels, which can be covered by stable oxides or metallic nanoparticles [1,2]. CFFs, due to conspicuous features such as chemical, mechanical, and thermal stabilities have been considerably regarded as bulk supports for large-scale catalyst synthesis [3–6]. Having a sizeable amount of parallel walls together with a porous framework has provided these structures with a potential for depositing catalytic active sites [7,8]. These properties enable CFFs to overcome intra-particle mass transfers and eliminate diffusions during the reaction process. In comparison to conventional networks, CFFs have higher flexibility in terms of surface functionalization [9]. In addition, the macroscopic nature of these structures facilitates their separation from the reaction mixture after the catalytic profile, which can improve their recyclability in further runs. Therefore, bulk CFFs can be considered a cost-effective and eco-friendly alternative for metallic and ceramic monolithic matrixes [10]. Despite these advantages, CFFs suffer significantly from their large dimensions and low surface area, which eventually results in reduced activity. Moreover, the ununiform distribution of CFFs pores will eventually result in a declined rate of durability in the case of final catalyst [11,12].

The idea of developing nitrogen-doped carbonaceous supports has been suggested for some time now, in an attempt to improve the CFFs' surface area and enhance their chemical activity [13–15]. Nitrogen atoms doped in carbonic materials, by having free lone pair electrons, can provide active coordination sites for metal nanoparticles through hydrophilicity, conductivity, and basicity inducing [16–18]. That is to say, the nitrogen species in modified CFFs are envisioned to create strong locations for better immobilization of metallic nanoparticles, leading to the suppression of unwanted aggregations [19]. Furthermore, the introduction of nitrogen atoms into the carbonaceous matrixes can potentially balance the electronic characteristics, handle the band gap energies, and charge density to the large extent [20,21]. Park and co-authors reported the immobilization of Cu-Pd alloy nanoparticles on the surface of graphitic carbon nitride by implementing the sol-gel method, by which high uniform dispersion of nanoparticles on the surface of g-C_3N_4 was achieved. The homogeneous distribution of particles together with the synergic effect between the support and active metals resulted in better hole-electron separation, which ultimately resulted in high solar energy conversion [22]. In-situ construction of nitrogen-doped CFFs during the direct incorporation of metallic nanoparticles has been regarded as an efficient technique in the construction of reusable bulk nanocatalysts. For example, in our previous work, we reported the construction of Co/N—CFF@TiO_2-SiO_2 nanocatalyst by using nitrogen-doped CFFs, which induced better textural, mechanical, and chemical properties in the final architecture. Besides, our synthetic strategy has significantly improved the electrical conductivity and

* Corresponding author.
E-mail address: sayyed.hosseini@alumni.iut.ac.ir (S.M. Hosseini).

https://doi.org/10.1016/j.mcat.2023.113736
Received 6 August 2023; Received in revised form 10 November 2023; Accepted 27 November 2023
Available online 5 December 2023

hydrophobicity of the optimized catalyst, which consequently the high selectivity and reasonable yield of acetophenone achieved upon aerobic ethylbenzene oxidation [23]. Copper-based catalysts containing CFFs decorated with nitrogen species exhibited good activity in pollutant reduction at room temperature, which was reported earlier. The study explained how modification of CFFs by impregnation method results in uniform distribution of copper nanoparticles. Employing green techniques and starting materials will enable the preparation of a final composite as a sustainable alternative and ideal platform for industrial wastewater treatment [24].

Herein, we implemented again the strategy to immobilize copper nanoparticles into the microfibers of CFFs during modification of fibers by nitrogen atoms, aiming to suppress active site leaching and achieve better catalyst separation. In this method, heteroatoms can be encapsulated into the CFFs through the thermal pyrolysis of a mixture of melamine and a widely-used cobalt (salen) complex. In the as-prepared composite, the nitrogen atoms have a superior ability to interact with CFFs through the formation of a conjugate π system. Generally, loading nitrogen atoms into the CFFs will induce a unique possibility, by which the support and deposited metal can interact effectively, and as a result, the redox transfers can be properly adjusted. In the following, the performance of the catalyst was examined in the benzene oxidation by using hydrogen peroxide as a green oxidant in mild conditions. Owing to the synergic effects between functionalized CFFs and copper species, the newly-fabricated nanocatalyst has prestigious physical and chemical properties alongside the desired catalytic activity. This profile can be extended as a novel route for the synthesis of embedded bulk catalysts for large-scale destinations. We believe that the macroscopic nature of the nanocatalyst gives it a unique capability for separation after successive reactions.

2. Experimental section

2.1. Chemicals and materials

Benzene, copper(II) nitrate hexa-hydrate $Cu(NO_3)_2.\ 6H_2O$, ethylenediamine ($NH_2CH_2CH_2NH_2$), 2,5-dimethylfuran (C_6H_8O), salicylaldehyde and melamine (2,4,6-triamino-1,3,5-triazine) were purchased from the Merck company. Carbon fiber felts (CFFs) was commercially obtained from the OJS Company (Belarus). Dichloromethane, acetonitrile (anhydrous, 99.8%), and hydrogen peroxide 25% were provided from Sigma-Aldrich. Ethanol and other solvents were used in analytical grade without any extra refinement.

2.2. Synthesis of N, N′-bis (salicylidene) ethylenediamine copper (II), Cu (salen) complex

N, N′-bis (salicylidene) ethylenediamine, known as salen ligand, was prepared according to the reports available in the literature [25]. For this purpose, 2 mmol of ethylenediamine were added dropwise into a round-bottom flask containing a mixture of 4 mmol of salicylaldehyde and 5 mL of ethanol at boiling point, which was followed by stirring for 2 h. After that time, the reaction mixture was cooled to obtain yellow crystals, filtered and purified by ethanol, and then dried in a vacuum oven at 60 °C overnight.

For the synthesis of Cu(salen) complex, on the one hand, a solution of 0.03 mol/L $Cu(NO_3)_2.\ 6H_2O$ in ethanol was prepared. On the other hand, the specific amount of newly-fabricated N, N-bis ethylene diamine (salen ligand) was dissolved in dichloromethane. Next, both solutions were mixed for 4 h under a nitrogen atmosphere. After completion, the precipitates were collected and washed with ethanol several times, and then the prepared sample was dried at 60 °C overnight.

2.3. Synthesis of Cu/N-CFF

Nitrogen-doped carbon network containing copper nanoparticles (Cu/N—CFF) was fabricated by the following method: Firstly, the pristine CFFs were washed in a mixture of water and ethanol under ultrasonic conditions, aiming to remove carbonic impurities, pollutants, and powdery residues from their surface. After cleaning, the bulk CFFs were dried at 80 °C for hours, and then were used as a firm support for copper complex stabilization. For this purpose, 500 mg of dry CFFs was shopped down into smaller pieces and distributed over 100 ml of water/ethanol (50/50) solution containing 12.5 g of the Cu (salen) complex and 250 mg of melamine. After stirring at 60 °C for 12 h, the solvent was then completely evaporated based on a well-known wet-impregnation method. After complete solvent evaporation, the solid was collected, calcined under nitrogen atmosphere at 550 °C temperature for 4 h, and finally named as Cu (20 wt%)/N—CFF nanocatalyst. Samples with copper contents of 10 and 40% were synthesized by a similar methodology, which were labeled as Cu (10 wt%)/N—CFF and Cu (40 wt %)/N—CFF catalysts respectively.

2.4. Catalytic performance reactions

Thermal oxidation of benzene-to-phenol was carried out by using hydrogen peroxide (25%) in a 50 mL autoclave batch system equipped with a digital gage and a thermometer to adjust the nitrogen pressure and temperature respectively. The reactor had also relevant input and output vents for charging and discharging the inert gas respectively. Typically, 50 mg catalyst and 5 ml acetonitrile as solvent were loaded into the reactor, followed by adding 2 ml of benzene and 2 ml of hydrogen peroxide (25%). Next, the reactor was pressurized up to 5 bar of N_2 gas to prevent the thermal decomposition of oxidant at the desired temperature and after adjusting the temperature to 80 °C, the oxidation was carried out for 6 h. After completion, the bulk catalyst was removed and the flask mixture was diluted by adding ethanol and a specific amount of an internal standard (acetophenone). Finally, the kind and the amount of products were evaluated by Gas Chromatography-Mass spectrometry and Gas Chromatography respectively.

2.5. Characterization

The XRD patterns of as-prepared nanocatalysts were measured by using an X-ray diffraction (XRD) equipment (Netherland) with Cu anode (40 kV, 30 mA) connected to a DACO-MP microprocessor using the Diffract-AT software in the range of $2\theta = 10^{\circ}-90^{\circ}$ Field emission scanning electron microscopy (FESEM) alongside with energy dispersive X-ray spectrometry (EDX) and mapping were recorded by implementing a TESCAN MIRA3 instrument (Japan). For such analysis, the bulk samples in their powdery forms were dusted on the surface of a tape and coated with a layer of gold to diminish charge turbulence. Thermogravimetric Analysis (TGA) was investigated by utilizing a TGA instrument (STA503 TA tool, Germany) in an argon atmosphere in the scanning range of 50–800 °C with a heating rate of 10 °C/min. BET-surface area measurements, as well as N_2 adsorption-desorption isotherms, were obtained at 77 K by applying a Micromeritics Digisorb 2600 system (Japan) instrument. The copper contents in the samples were determined by inductively-coupled plasma optical emission spectroscopy (ICP-OES) using a Shimadzu ARL 34,000 (Japan) instrument. In this case, the amount of 100 mg of catalyst (fresh sample or re-used catalyst) was digested in 50 mL of HNO_3/HCl (1/3 molar ratio) solution. The precise size, morphology, and distribution pattern of the Cu nanoparticles were determined by using a Philips CM-120 microscopy TEM instrument with an accelerating voltage of 150 kV. X-ray photoelectron spectroscopy (XPS) was performed by VG ESCALAB 3 MK II equipment. The measurement chamber pressure was $<10–9$ Torr and the samples were excited by using a monochromatic source of Mg Kα (1253.6 eV) radiation (operated at 300 W), having an instrument resolution of 0.7 eV. Moreover, the component peaks were separated by the Origin-pro software.

3. Results and discussion

3.1. FESEM and TEM

Field Emission Scanning Electron Microscopy (FESEM) surface graphs were measured to investigate the morphological features of pure CFFs and the distribution pattern of Cu (X wt.%)/N—CFF (X = 10, 20 and 40) catalysts. As can be seen from Fig. S1, pristine CFFs have smooth surfaces and fibers with micrometric diameters in different orientations. After Cu (20 wt.%)/N—CFF nanocatalyst construction, an un-uniform coverage of a carbonic network containing nano-metric spots was observed around the fibers (Fig. 1). Regarding EDX and mapping measurements, a uniform distribution of copper and nitrogen elements can be detected over the surface of CFF, which confirms the good potential of N—CFF for homogeneous dispersion of metallic sites. Plus, nitrogen atoms exist together with copper nanoparticles in the modified carbonic framework (Fig. S2).

Transmission Electron Microscopy (TEM) images of Cu (20 wt.%)/N—CFF nanocatalyst in Fig. 2, in addition, illustrate the homogeneous dispersion of nano-scale particles of copper with different sizes (dark spots) over the surface of nitrogen-doped CFFs. Some particles with an average size of less than 100 nm can be detected, which probably contributed to the metallic copper nanoparticles or metal oxide (see Section 3.6 for XPS data) deposited on the nitrogen-doped carbon matrix. In Fig. 2 the bright background can be related to the modified CFFs, whereas the salient spots that appeared on the CFFs surface are possibly concerned with copper nanoparticles. It is claimed that through thermal condensation, the copper nanoparticles decorated into the N-doped framework, were completely attached to the underlying support, through nitrogen coordination, which leads to the prevention of metal leaching during the catalytic test (see Fig. S2 and Table S1). Despite the Cu (20 wt.%)/N—CFF nanocatalyst, the sample with larger amounts of copper metal didn't show the homogenous distribution of copper nanoparticles. Figure S3 demonstrates the FESEM graphs of Cu (40 wt.%)/N—CFF catalyst (c-d) alongside the images of Cu (10 wt.%)/N—CFF sample (a-b) in different magnifications. By treating the carbon fibers via 10 wt.% of copper-containing ligands, nitrogen-doped matrixes appeared on the surface of microfibers without changing the integrity of CFF structure (Fig. 3) Based on these graphs, the networks penetrate into the matrix of fibers and are just deposited on the CFFs as a smooth surface. By enhancing the weight percentage of Cu(salen), big agglomerates of Cu-N units were locally investigated on the surface of CFFs. This claim can be approved by investigating the morphology of catalysts by TEM characterization, by which the immobilization of copper particles with larger diameter (mean size of 26.22 nm) in the Cu (40 wt.%)/N—CFF catalyst can be observed (Figs. S4 and S5).

3.2. BET analysis

Textural properties and nitrogen adsorption-desorption isotherm of pristine CFFs and Cu (20 wt.%)/N—CFF nanocatalyst were examined by Brunauer-Emmett-Teller (BET) measurement. There is a steady increase in the N_2 adsorption-desorption of CFFs isotherm during the enhancement of P/P_0 amount, which is the characteristic feature of CFFs macroporous structures. This is the direct result of complete single-layers and multi-layers' adsorption without any hysteresis loop. According to the IUPAC standards, CFFs could be classified as macro-porous material (Fig. S6) [26]. Considering the Cu (20 wt.%)/N—CFF nanocatalyst, the adsorption started at low pressure with a slight uptake, followed by a sharp rise in the adsorption at higher pressures. Having H_2 type hysteresis loop as well as the isotherm of IV type recommends a mesoporous structure for optimized Cu (20 wt.%)/N—CFF nanocatalyst (Fig. S7). Furthermore, the results of BET analysis show that the optimized Cu (20 wt.%)/N—CFF nanocatalyst has an improved rate of surface area and pore volume compared to the pristine CFFs (Table S2). This improvement in textural properties can be related to the modification of CFFs through the nitrogen doping process. The enhanced surface area that is resulted from the modification strategy is of paramount importance for catalyst performance during oxidation reaction as well as improving the adsorption and desorption of reactants and products to and from catalytic sites respectively.

3.3. Raman shift analysis

This measurement was performed to collect the Raman spectra of pure CFFs and catalysts containing different percentages of copper nanoparticles. The investigation has a great potential to evaluate the amount of orders and disorders in modified carbonic material near the

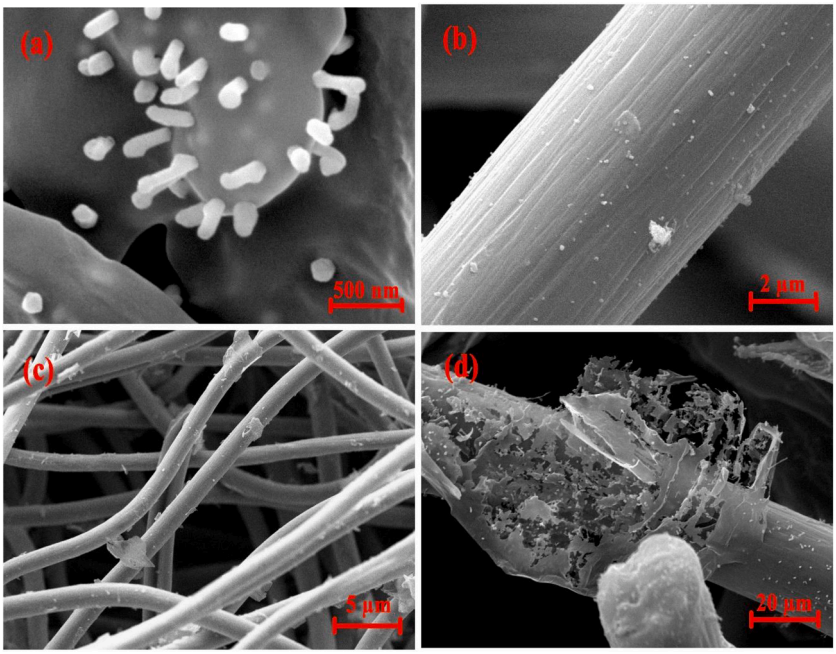

Fig. 1. FESEM images of Cu (20 wt.%)/N—CFF nanocatalyst in different magnifications (a-d).

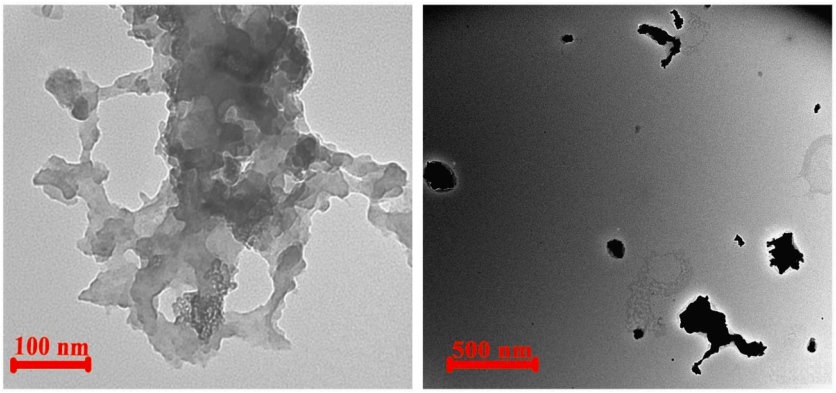

Fig. 2. TEM graphs of Cu (20 wt.%)/N—CFF nanocatalyst.

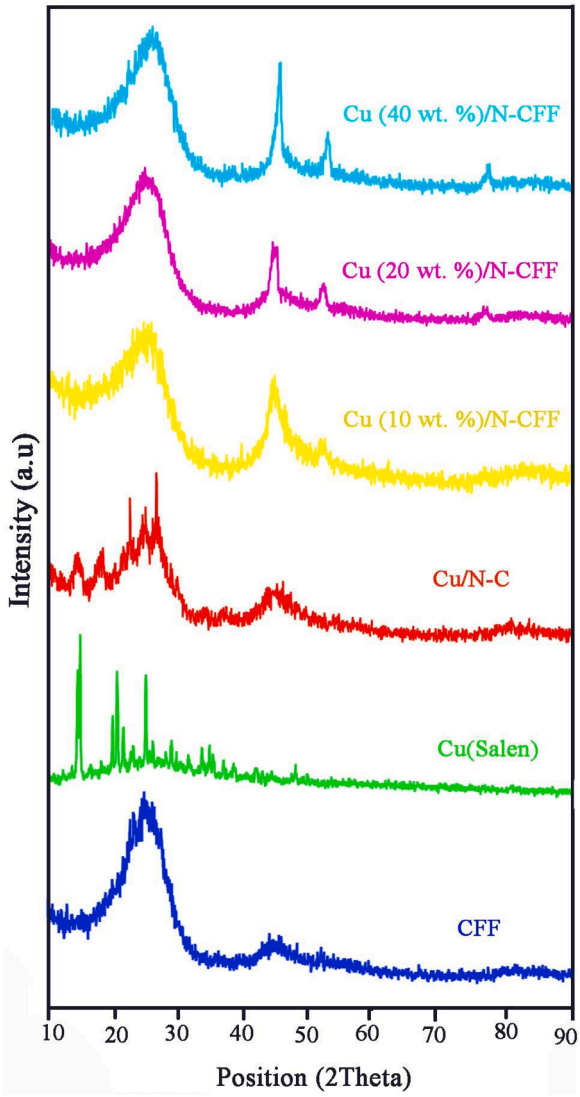

Fig. 3. XRD patterns of CFFs (blue), Cu(salen) (green), Cu/N—C (red), Cu (10 wt.%)/N—CFF (yellow), Cu (20 wt.%)/N—CFF (purple), and Cu (40 wt. %)/N—CFF (turquoise) (For interpretation of the references to color in this figure legend, the reader is referred to the web version of this article.).

surface. Due to the stress experienced at various carbonic moieties and crystalline size, two separate bands with distinguished frequency and intensity is expected. As it can be seen from Fig. S8, the pure CFFs in the range of 1000–1800 cm^{-1} exhibited D band at 1361 cm^{-1} which shows the carbonic moieties with amorphous phase containing activated functional groups and structural defects. Another peak at 1592 cm^{-1} which is known as G band, belongs to the carbon atoms with S_P^2 hybridization. This peak has the vibrational characteristic of S_P^2 carbon atoms connected to the graphite layers. After functionalization and catalysts construction, it can be clearly observed that the position of major peaks for CFFs has not changed, which explains that the nitrogen doping strategy cannot alter the final morphology and whole integrity of the CFFs. The amount of disorders in the Cu (X wt.%)/N—CFF ($X = 10$, 20 and 40) was found to be slightly larger after metal loading and thermal treatment, when compared to the pristine CFFs. Looking at the details, there is an increase in the I_D/I_G ratio of catalysts by growing in the amount of copper percentage, meaning that the Cu (40 wt. %)/N—CFF catalyst has the lowest amount of orders (Table S3). The data confirms appearing of more disorders or probably more interaction between CFFs and Cu/N—C unites after thermal condensations, which agrees properly with our previous characterizations (see Section 3.1 for microscopy analysis).

3.4. TGA and ICP-OES studies

Thermal properties of Cu (20 wt.%)/N—CFF nanocatalyst was recorded by applying Thermogravimetric Analysis (TGA) measurement in the range of 50–800 °C temperature in an argon atmosphere. As the weight loss of less than 5% for Cu (20 wt.%)/N—CFF sample was observed below 400 °C, the nanocatalyst is believed to have a good stability in moderate temperatures. The earlier decline in the weight loss of catalyst below 400 °C can be attributed to the water loss and organic functional group elimination (Fig. S9). The further weight loss (less than 10%) observed in the TGA of catalyst between 400 and 600 °C is related to the partial degradation of organic framework and condensation of N-doped structure. The better stability of Cu (20 wt.%)/N—CFF nanocatalyst compared to CFFs can be explained by the fact that the TGA curve of un-modified CFFs has illustrated the weight loss of more than 30% at 600 °C under same measurements (Fig. S9). It appears to be a reasonable conclusion that the nitrogen doping process for CFFs and subsequent immobilization has led to the better thermal resistance than pristine CFFs. In addition to the better thermal stability obtained by TGA analysis, the modification technique seems to have a profound impact on the mechanical stability of as-prepared nanocatalyst, so that the data of inductively-coupled plasma optical emission spectroscopy (ICP-OES) can prove our argument. Table S1 demonstrates that the Cu (20 wt. %)/N—CFF consists of just 2.7 percentage of copper, while after nine cycles of reaction the value has had a slight diminish. This observation illustrates that the Cu (20 wt.%)/N—CFF nanocatalyst has kept its stability during the oxidation reaction.

3.5. XRD studies

X-ray diffraction patterns of CFFs and Cu (X wt.%)/N—CFF ($X = 10$, 20 and 40) catalysts during each stage of synthetic protocol are showed in Fig. 3. Pristine CFFs shows two broad peaks at 25° and 43°, which are related to the (002), and (001) planes of amorphous CFFs respectively. By the thermal condensation of Cu (salen) complex with CFF, the decoration of copper/copper oxide nanoparticles into the carbonic matrix were occurred (Cu/N—CFF). In this case the peaks in 43.3°, 50.4°, and 74.1° can be observed, which belongs to the crystalline planes of copper (planes of 111, 200, and 220 respectively, based on JCPDS No. 04-0836) [27–29]. The Cu/N—CFF structures shows generally an amorphous pattern, which is highly similar to the pattern of pristine CFFs. This observation explains that the modification strategy through doping nitrogen atoms had no significant effect on the whole integrity of CFFs matrix. XRD patterns including some well-recognized peaks of catalysts containing different copper contents Cu (10, 20 and 40 wt. %)/N—CFF are observed in Fig. 3. Obviously, by increasing the percentage of copper in the final catalyst an enhancement in the intensity of Cu characteristic peaks and subsequent crystallinity can be detected.

3.6. XPS studies

X-ray photoelectron spectroscopy (XPS) was performed to study the chemical composition of surface and determine the oxidation states of metallic atoms in the optimized nanocatalyst. Fig. S10 and Table S4 demonstrates the wide scan survey of Cu (20 wt.%)/N—CFF nanocatalyst as well as surface concentration of carbon, oxygen, nitrogen, and copper elements. The deconvoluted spectra for carbon 1S illustrate two distinguished peaks at 284–285.1 and 287.6 eV, which are related to the C—H/C—C, and C=O bonds respectively (Fig. 4, left). Regarding the O 1S core, the fragments of N—C-O and C=O show their specific peaks at 531.5 eV and 532.9 eV respectively (Fig. 4, right). In addition, the O 1S deconvoluted spectra of Cu (20 wt.%)/N—CFF nanocatalyst demonstrates the copper oxide peak at 529.5 eV.

Based on our previous works [24], the nitrogen atoms in an N—CFF can be seen in various forms such as pyridinic, pyrrolic, oxidized nitrogen (N—Oxide), and quaternary ones. In the deconvoluted spectra of N 1s, two main peaks appeared at 401.2 eV and 398.8 eV, which can be assigned to C—N (pyrrolic- nitrogen) and N—Cu pieces. According to our measurements nowhere can be found the characteristic peaks of oxidized nitrogen, quaternaries and pyrrolic ones (Fig. 5, left). Considering copper atom, there are two prominent peaks in the spectrum of Cu core in the binding energies of 932.8 eV (Cu 2p3/2) and 952.9 eV (Cu 2p1/2), which can be attributed to the Cu2O specie. Indeed, the peaks at 934 eV and 954 eV together with the broad satellite peaks around 934–947 eV confirm the presence of Cu(II) species (Fig. 5, right) [30]. The presence of copper cations can be explained by the possible oxidation of metal salts during the condensation or exposure to the air.

3.7. Catalysts performance

To examine the catalytic activity of various catalysts prepared by the strategy, the catalysts were tested in direct oxidation of benzene-to-phenol (by utilizing H_2O_2 25% as a cost-effective and environmentally-friendly oxidizing agent) under mild thermal conditions (Fig. 6).

The obtained results for Cu (X wt.%)/N—CFF ($X = 10$, 20, and 40) catalysts and other materials are shown in Table 1. For this, the reaction flask was firstly charged with 5 bar of nitrogen gas to prevent oxidant decomposition at high temperatures. Table 1 depicted the data of reactions in acetonitrile as solvent, followed by determining the exact amounts of products by gas chromatography. Cu (X wt.%)/N—CFF catalysts ($X = 10$, 20, and 40) showed better activity toward selective phenol production compared to the un-calcined samples (Table 1, Entries 5–7 compared to 1–4 ones). The reason behind this story is associated with the pyrolysis effect, in which the releasing of active sites of Cu/N—CFF will lead catalytic sites to be more accessible for the oxidation reaction [31]. When the Cu-Salen/CFF and N—CFF structures were tested, the amounts of phenol were negligible, as yields of 3 and 1% were found respectively. Clearly, for CFFs and salen/CFF no catalytic activity was observed, and thus no phenol production as well. To investigate the effect of the presence of CFF as support catalyst sample without CFF (Cu/N—C) was also produced under same condition. The structure showed low activity and selectivity toward phenol production (12 and 62% for phenol yield and selectivity respectively, (Table 1, Entry 5). As expected, the increase in the amount of copper content up to 20% can lead to the higher rate of activity, after which a sharp decline in the figure can be observed for higher copper percentages (Table 1, Entry 6–8). One explanation for this behavior is that a higher weight percent of Cu(salen) used during catalyst construction was found to cause higher yields of di-hydroxylated isomers and lower selectivity towards phenol as the main product, meaning that the lower amounts of copper are preferable for achieving high selectivity of phenol. This is because the as-prepared phenol is believed to be oxidized more actively (compared with starting benzene) by remaining oxidants and catalysts in the reactor [18,23]. To evaluate the effect of the type of oxidant on the activity of catalyst during oxidation, molecular oxygen as an inexpensive and environmentally-friendly reagent was investigated. Based on the results, no amount of phenol product detected by our experiment. Higher temperature is observed to cause in phenol production by lower selectivity. The reduction in selectivity in harsh condition give rise to more by-products at higher temperature (Table 1, Entries 9 and 10).

To study the effect of various parameters on the oxidation progress, different factors were investigated in the presence of Cu (20 wt. %)/N—CFF nanocatalyst by using 25% hydrogen peroxide. According to

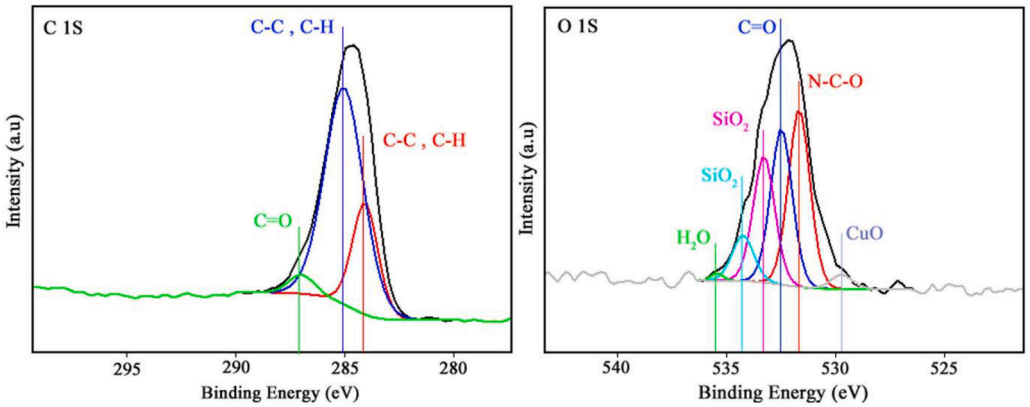

Fig. 4. XPS deconvoluted spectrum of Cu (20 wt.%)/N—CFF nanocatalyst at the core levels of C 1s (left) and O 1S (right).

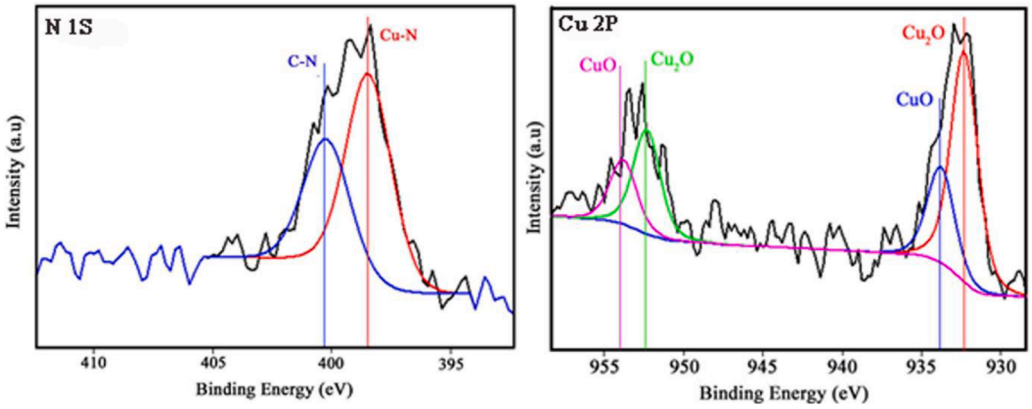

Fig. 5. XPS deconvoluted spectrum of Cu (20 wt.%)/N—CFF nanocatalyst at the core levels of N 1s (left) and Cu 3P (right).

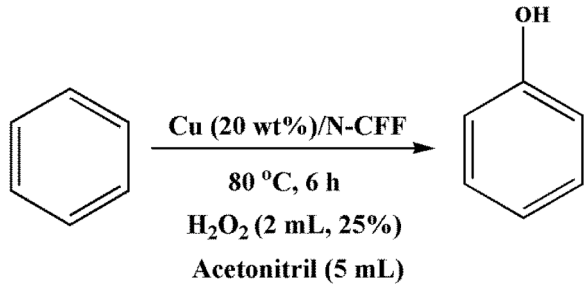

Fig. 6. Pathway for benzene-to-phenol oxidation in the presence of Cu (20 wt %)/N—CFF nanocatalyst.

Table 1
Catalytic activity of various catalysts during oxidation of benzene.

Entry [a]	Type of Catalyst	PhOH Yield (%)	PhOH Selectivity (%)	TOF [b] (h^{-1})
1	CFF	–	–	–
2	Salen-CFF	–	–	–
3	N-CFF	>1	>1	>1
4	Cu-Salene/CFF	3	54	1
5	Cu/N—C	12	62	4.3
6	Cu(10 w%)/N—CFF	17.5	95	6.4
7	Cu(20 w%)/N—CFF	25.2	100	9.2
8	Cu(40 w%)/N—CFF	14.3	76	5.2
9[c]	Cu(20 w%)/N—CFF	–	–	–
10[d]	Cu(20 w%)/N—CFF	5	35	1.8

[a] : Bz and PhOH stands for benzene and phenol respectively. Reaction conditions: Acetonitrile (5 ml) as solvent, Temperature of 80 °C, 6 h time of reaction, H_2O_2 (25%) as oxidant, H_2O_2/Bz molar ratio of 4, 2 ml of Benzene, Temperature of pyrolysis: 550 °C and 25 mg of catalyst.

[b] : b. *The number of moles of the substrate (benzene) converted to main product (phenol) per hour, per mole of the used metal catalyst was defined as TOF.

[c] : Bz and PhOH stands for benzene and phenol respectively. Reaction conditions: Acetonitrile (5 ml) as solvent, Temperature of 80 °C, 6 h time of reaction, 15 bar pressure of O_2, 2 ml of Benzene, Temperature of pyrolysis: 550 °C and 25 mg of catalyst.

[d] : Bz and PhOH stands for benzene and phenol respectively. Reaction conditions: Acetonitrile (5 ml) as solvent, Temperature of 120 °C, 6 h time of reaction, 15 bar pressure of O_2, 2 ml of Benzene, Temperature of pyrolysis: 550 °C and 25 mg of catalyst.

the optimized conditions, the highest selectivity and a reasonable yield of phenol were achieved in 5 mL acetonitrile, 80 °C temperature, 6 h time of reaction, 25 mg of catalyst, and benzene/H_2O_2 molar ratio of 4. Higher temperatures were demonstrated to yield lower amounts of main product, and thus less selectivity, which means that more by-products can probably be formed [31]. This is due to the fact that the phenol is always estimated to be over-oxidized more easily than benzene in the presence of remnant oxidant and active catalyst. This is in agreement with literature, in which the higher temperatures can perhaps lead to the benzene over-oxidation, or even phenol degradation, meaning that lower temperatures are preferable to obtain higher products (Table 2, Entries 1–5) [32]. Considering the highest amount of phenol yield and selectivity, the optimized reaction temperature is selected as 80 °C (Table 2, Entry 2). Table 2 demonstrate the phenol yield and selectivity of reaction by changing the amount of catalysts and a similar trend to the temperature optimization can be observed in the range of 25–150 mg (Entries 6–8). The findings clearly showed that the highest activity can be achieved by using 25 mg of Cu (20 wt.%)/N—CFF nanocatalyst, so that in the presence of higher amounts of catalyst, more by-products were detected. Due to some operational limitations in our laboratory, it was found unaffordable to try with the catalyst amounts less than 25 mg. Once the molar ratio of H_2O_2/Benzene was investigated, it was found that the initial increase in the ratio led to a higher activity in the selective production of phenol, after that, the amount was sharply reduced. This is due to the fact that an extra amount of oxidant is imagined to oxidize the newly-generated phenol, providing other by-products, as mentioned earlier. (Table 2, Entries 9–11) [18–23]. As expected, the catalyst illustrated superior performance after thermal treatment in extreme conditions, compared to the samples prepared before pyrolysis. To evaluate the suitable conditions for achieving the highest amounts of phenol, composites containing 20 wt.% of copper were calcined at different temperatures. The catalysts which were subjected to calcination at 450 °C and 550 °C temperatures had the better yield and selectivity for phenol compared to the catalyst treated at 650 °C (Table 2, Entries 12–13). At optimized parameters and maintaining other parameters, some experiments were carried out to study the impact of different times of reaction on the oxidation reaction.

The data in Fig. S11 shows that no remarkable effect of time periods was expected on the reaction process during our experiments (that was altered from 3 to 18 h) and the results were changed from 8.7 to 9.2 and 22.3–25.2 for TOF and yield of phenol respectively. In addition to that, the reusability of Cu (20 wt.%)/N—CFF nanocatalyst was studied over ten successive reactions. For this investigation, the recycled sample was removed from the batch reactor and after washing with a mixture of water-ethanol, the sample was applied for further runs. The results demonstrated that the yield of phenol was dropped by 0.5–1%, from 25.2 in the first cycle to 24.8 in the ninth run, whereas at the same time the selectivity for phenol product remained mostly stable (Fig. 7). To explain this observation, it can be proposed that the simultaneous doping of nitrogen atoms to the CFFs and deposition of copper nanoparticles into the as-prepared N—CFF can prevent conventional aggregations (see Section 3.1) and avoid leaching (see data in the Table S1) of metallic particles during the oxidation process. This is in complete

Table 2
Effect of different reaction parameters on the catalytic activity of Cu (20 wt.%)/N—CFF nanocatalyst during the oxidation of benzene.

Entry [a]	Temperature (°C)	Amount of Catalyst (mg)	H_2O_2/Bz ratio	Pyrolysis Temperature (°C)	PhOH Yield (%)	PhOH Selectivity (%)	TOF [b] (h^{-1})
1	60	25	4	550	13.3	88	4.9
2	80	25	4	550	25.2	100	9.2
3	100	25	4	550	22.4	99	8.2
4	110	25	4	550	23.5	99	8.8
5	120	25	4	550	22.5	98	8.1
6	80	50	4	550	20	92	7.8
7	80	100	4	550	19.2	88	7.4
8	80	150	4	550	14.9	52	5.3
9	80	25	1	550	16.4	63	6.2
10	80	25	2	550	18.4	83	7.1
11	80	25	6	550	15.1	65	5.4
12	80	25	4	450	18.2	89	6.1
13	80	25	4	650	15.9	78	5.6

[a] : Bz and PhOH stands for benzene and phenol respectively. All the tests were carried in acetonitrile (5 ml) as solvent, 6 h time of reaction and H_2O_2 (25%) as oxidant.
[b] : b. *The number of moles of the substrate (benzene) converted to main product (phenol) per hour, per mole of the used metal catalyst was defined as TOF.

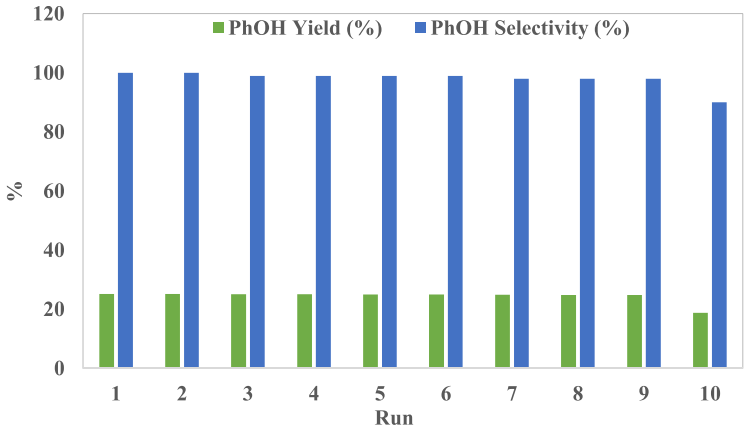

Fig. 7. The reusability of Cu (20 wt.%)/N—CFF nanocatalyst.
Note: PhOH stands for phenol. Reaction conditions is: Acetonitrile (5 ml) as solvent, Temperature of 80 °C, 6 h time of reaction, H_2O_2 (25%) as oxidant, H_2O_2/Bz molar ratio of 4, 2 ml of Benzene, Temperature of pyrolysis: 550 °C and 25 mg of catalyst.

agreement with ICP-OES (Table S1) and EDX-Mapping (Fig. S2) results, in which the strong coordination of copper metals (see also Fig. 5 to find Cu-N sites) to the active nitrogen sites as well as distribution over the mesoporous framework potentially hindered metal nanoparticles to stand out of the whole matrix. Nevertheless, for 10th run the phenol yield and selectivity dropped to 18.8 and 90% respectively. This can be related to the loss of some active metal centers (Table S1) as well as particle aggregation during recyclability reactions. The TEM images of catalyst after reaction illustrate the particles with average size larger than 100 nm for Cu (20 wt.%)/N—CFF catalyst (Fig. S12).

In the end, the performance of Cu (20 wt.%)/N—CFF nanocatalyst was compared with the similar reports in the literature [32–40]. Even though the comparison between the data does not appear to be logical because of the differences in reaction conditions, it seems to be a reasonable conclusion that the Cu (20 wt.%)/N—CFF nanocatalyst has an acceptable yield and excellent selectivity in mild reaction conditions. Besides, the catalyst due to its macroscopic nature, can be considered a wonderful alternative for industrial applications (Table S5).

4. Conclusion

In summary, we developed a co-assembly profile for the synthesis of a heterogeneous bulk nanocatalyst based on a porous nitrogen-doped CFFs support during the immobilization of copper nanoparticles. The structural, morphological, and textural characterizations demonstrated that the Cu (20 wt.%)/N—CFF nanocatalyst has outstanding performance in one-pot thermal oxidation of benzene-to-phenol in mild conditions. The characterization of the newly-fabricated catalyst confirmed that copper nanoparticles have a relatively narrow size distribution over the macroscopic framework. These features prove that the optimized composite has strong mechanical, textural, and thermal features, preventing metal from leaching, thus leading to a higher lifetime. The optimized catalyst in ideal conditions in the presence of 25% H_2O_2 as a low-cost and environmentally-friendly oxidant, acetonitrile as the solvent, and nitrogen gas as an inert atmosphere showed the amounts of 25.2 and 100% for phenol yield and selectivity respectively. Due to its noticeable structural properties, the Cu (20 wt.%)/N—CFF nanocatalyst maintained its activity (phenol yield and selectivity) for nine consecutive cycles, whereas the yield and selectivity just dropped to 18.8 and 90% in tenth cycle respectively. Finally, because of the bulk nature of Cu (20 wt.%)/N—CFF nanocatalyst and its durability, it can be concluded that the designed nano-composite can be regarded as a useful candidate in large-scale applications.

Author contribution statement

Mis. Somayeh TavasoliKejani: Graduate student which has done the experiments and written the article.

Dr. Sayyed Mahdi Hosseini: He is the corresponding author and has edited the manuscript.

Professor Mehran Ghiaci: Defined the work, and supervised the research.

Mis. Thomas Vangijzegem: Helped us to get XPS spectra of the catalysts, and the TEM images.

Professor Sophie Laurent: Helped us to get XPS spectra of the catalysts, and the TEM images.

Supporting information

- Additional characterization data related to the optimized catalyst and support
- Additional data related to the optimization reactions

Declaration of Competing Interest

The authors declare that they have no known competing financial interests or personal relationships that could have appeared to influence the work reported in this paper.

Data availability

The data that has been used is confidential.

Acknowledgments

The authors thank the Isfahan University of Technology for financial support and University of Mons for technical support.

Supplementary materials

Supplementary material associated with this article can be found, in the online version, at doi:10.1016/j.mcat.2023.113736.

References

[1] W.Y. Hong, S.P. Perera, A.D. Burrows, Manufacturing of metal-organic framework monoliths and their application in CO_2 adsorption, Microporous Mesoporous Mater. 214 (2015) 149–155, https://doi.org/10.1016/j.micromeso.2015.05.014.
[2] S.B. Tasi, H.A. Ma, Research on preparation and of the monolithic catalyst with interconnecting pore structure, Sci. Rep. 8 (2018) 16605–16614, https://doi.org/10.1038/s41598-018-35021-2.
[3] S.G. Mohammad, S.M. Ahmed, Preparation of environmentally friendly activated carbon for removal of pesticide from aqueous media, Int. J. Ind. Chem. 8 (2017) 121–132, https://doi.org/10.1007/s40090-017-0115-2.
[4] S. Ge, Z. Liu, Y. Furuta, W. Peng, Characteristics of activated carbon remove sulfur particles against smog, Saudi J. Biol. Sci. 24 (2017) 1370–1374, https://doi.org/10.1016/j.sjbs.2016.12.016.
[5] C. Huang, Q. Zhang, T. Chou, C. Chen, D.S. Su, R. Doong, Three-dimensional hierarchically ordered porous carbons with partially graphitic nanostructures for electrochemical capacitive energy storage, ChemSusChem 5 (2012) 563–571, https://doi.org/10.1002/cssc.201100618.
[6] A. Ghosh, Y.H. Lee, Carbon-based electrochemical capacitors, ChemSusChem 5 (2012) 480–499, https://doi.org/10.1002/cssc.201100645.
[7] Y. Lv, X. Tan, F. Svec, Preparation and applications of monolithic structures containing metal–organic frameworks, J. Sep. Sci. 40 (2017) 272–287.
[8] T. Boger, Monolithic catalysts for the chemical industry, Ind. Eng. Chem. Res. 43 (2004) 4602–4611, https://doi.org/10.1021/ie030730q.
[9] K.P. de Jong, J.W. Geus, Carbon nanofibers: catalytic synthesis and applications, Catal. Rev. 42 (2007) 481–510, https://doi.org/10.1081/CR-100101954.
[10] J. Williams, Monolith structures, materials, properties and uses, Catal. Today 69 (2001) 3–9, https://doi.org/10.1016/S0920-5861(01)00348-0.
[11] A. Cybulski, J.A. Moulijn, Monoliths in heterogeneous catalysis, Catal. Rev. 36 (1994) 179–188, https://doi.org/10.1080/01614949408013925.
[12] E. Perez-Mayoral, V. Calvino-Casilda, E. Soriano, Metal-supported carbon-based materials: opportunities and challenges in the synthesis of valuable products, Catal. Sci. Technol. 6 (2016) 1265–1291, https://doi.org/10.1039/C5CY01437A.
[13] L. Zhao, L. Fan, M. Zhou, H. Guan, S.Y. Qiao, M. Antonietti, Nitrogen-containing hydrothermal carbons with superior performance in supercapacitors, Adv. Mater. 22 (2010) 5202–5206, https://doi.org/10.1002/adma.201002647.
[14] L.F. Chen, X.D. Zhang, H.W. Liang, M.G. Kong, Q.F. Guan, P. Chen, Z.Y. Wu, S. H. Yu, Synthesis of nitrogen-doped porous carbon nanofibers as an efficient electrode material for supercapacitors, ACS Nano 6 (2012) 7092–7102, https://doi.org/10.1021/nn302147s.
[15] Q. Shi, R.Y. Zhang, Y.Y. Lv, Y.H. Deng, A.A. Elzatahrya, D.Y. Zhao, Nitrogen-doped ordered mesoporous carbons based on cyanamide as the dopant for supercapacitor, Carbon N Y 84 (2015) 335–346, https://doi.org/10.1016/j.carbon.2014.12.013.
[16] S. Nilforoushan, M. Ghiaci, S.M. Hosseini, S. Laurent, R.N. Muller, Selective liquid phase oxidation of ethyl benzene to acetophenone by palladium nanoparticles immobilized on a g-C_3N_4–rGO composite as a recyclable catalyst, New J. Chem. 43 (2019) 6921–6931, https://doi.org/10.1039/C8NJ06469E.
[17] J. Hao, J. Wang, S. Qin, D. Liu, Y. Li, W. Lei, B/N co-doped carbon nanosphere frameworks as high-performance electrodes for supercapacitors, J. Mater. Chem. A 6 (2018) 8053–8058, https://doi.org/10.1039/C8TA00683K.
[18] S.M. Hosseini, M. Ghiaci, A.A. Kulinich, W. Wunderlich, H. Farrokhpour, M. Saraji, A. Shahvar, Au-Pd@g-C_3N_4 as an efficient photocatalyst for visible-light oxidation of benzene to phenol: experimental and mechanistic study, J. Phys. Chem. C 122 (2018) 27477–27485, https://doi.org/10.1021/acs.jpcc.8b08788.
[19] T. Horikawa, N. Sakao, T. Sekida, J. Hayashi, D.D. Do, M. Katoh, Preparation of nitrogen-doped porous carbon by ammonia gas treatment and the effects of N-doping on water adsorption, Carbon N Y 50 (2012) 1833–1842, https://doi.org/10.1016/j.carbon.2011.12.033.
[20] P. Zhang, F. Sun, Z. Xiang, Z. Shen, J. Yun, D. Cao, ZIF-derived in situ nitrogen-doped porous carbons as efficient metal-free electrocatalysts for oxygen reduction reaction, Energy Environ. Sci. 7 (2014) 442–450, https://doi.org/10.1039/C3EE42799D.
[21] S. Wang, X. Zhao, T. Cochell, A. Manthiram, Nitrogen-doped carbon nanotube/graphite felts as advanced electrode materials for vanadium redox flow batteries, J. Phys. Chem. Lett. 3 (2012) 2164–2167, https://doi.org/10.1021/jz3008744.
[22] S.J. Park, Y. Zhang, Stabilizing CuPd bimetallic alloy nanoparticles deposited on holey carbon nitride for selective hydroxylation of benzene to phenol, J. Catal. 379 (2019) 154–163, https://doi.org/10.1016/j.jcat.2019.09.032.
[23] S.M. Hosseini, M. Ghiaci, S.A. Kulinich, W. Wunderlich, H. Ghaziaskar, A. J. Koupaei, Ethyl benzene oxidation under aerobic conditions using cobalt oxide embedded in nitrogen-doped carbon fiber felt wrapped by spiral TiO_2-SiO_2, Appl. Catal. A 630 (2022) 118456–118462, https://doi.org/10.1016/j.apcata.2021.118456.
[24] A. Shahzeydi, M. Ghiaci, L. Jameie, M. Panjepour, Immobilization of N-doped carbon porous networks containing copper nanoparticles on carbon felt fibers for catalytic applications, Appl. Surf. Sci. 485 (2019) 194–203, https://doi.org/10.1016/j.apcata.2021.118456.
[25] P. Karandikar, K.C. Dhanya, S. Deshpande, A.J. Chandwadkar, S. Sivasanker, M. Agashe, Cu/Co-salen immobilized MCM-41: characterization and catalytic reactions, Catal. Commun. 5 (2004) 69–74, https://doi.org/10.1016/j.catcom.2003.11.015.
[26] P.B. Balbuena, K.B. Gubbins, Theoretical interpretation of adsorption behavior of simple fluids in slit pores, Langmuir 9 (1993) 1801–1814, https://doi.org/10.1021/la00031a031.
[27] Q. Xu, B. Cheng, J. Yu, G. Liu, Making co-condensed amorphous carbon/g-C_3N_4 composites with improved visible-light photocatalytic H_2-production performance using Pt as cocatalyst, Carbon N Y 118 (2017) 241–249, https://doi.org/10.1016/j.carbon.2017.03.052.
[28] Y. Shi, Z. Yang, Y. Liu, J. Yu, F. Wang, J. Tong, B. Sua, Q. Wang, Fabricating a g-C_3N_4/CuOx heterostructure with tunable valence transition for enhanced photocatalytic activity, RSC Adv. 6 (2016) 39774–39783, https://doi.org/10.1039/C6RA04093D.
[29] G. Shi, L. Yang, Z. Liu, X. Chen, J. Zhou, Y. Yu, Photocatalytic reduction of CO_2 to CO over copper decorated g-C_3N_4 nanosheets with enhanced yield and selectivity, Appl. Surf. Sci. 427 (2018) 1165–1173, https://doi.org/10.1016/j.apsusc.2017.08.148.
[30] D.A. Bulushev, A.L. Chuvilin, V.I. Sobolev, S.G. Stolyarova, Y.V. Shubin, I. P. Asanov, A.V. Ishchenko, G. Magnani, M. Riccò, A.V. Okotrub, L.G. Bulusheva, Copper on carbon materials: stabilization by nitrogen doping, J. Mater. Chem. A 5 (2017) 10574–10583, https://doi.org/10.1039/C7TA02282D.
[31] S.M. Hosseini, M. Ghiaci, S. Kulinich, W. Wunderlich, B.H. Monjezi, Y. Ghorbani, H.S. Ghaziaskar, A.J. koupaei, Au-Pd nanoparticles enfolded in coil-like TiO_2 immobilized on carbon fibers felt as recyclable nanocatalyst for benzene oxidation under mild conditions, Appl. Surf. Sci. 506 (2020), 144644, https://doi.org/10.1016/j.apsusc.2019.144644.
[32] T. Jiang, W. Wang, B. Han, Catalytic hydroxylation of benzene to phenol with hydrogen peroxide using catalysts based on molecular sieves, NJC 37 (2013) 1654–1664, https://doi.org/10.1039/C3NJ41163J.
[33] A. Tabler, A. Hausser, E. Roduner, Aerobic one-step oxidation of benzene to phenol on copper exchanged HZSM5 zeolites: a mechanistic study, J. Mol. Catal. 379 (2013) 139–145, https://doi.org/10.1016/j.molcata.2013.08.012.
[34] P. Devaraji, N. Sathu, Ch. Gopinath, Ambient oxidation of benzene to phenol by photocatalysis on Au/$Ti_{0.98}V_{0.02}O_2$: role of holes, ACS. Catal. 9 (2014) 2844–2853, https://doi.org/10.1021/cs500724z.
[35] Z. Long, Y. Zhou, G. Chen, W. Ge, J. Wang, C3N4-H5PMo10V2O40: a dual-catalysis system for reductant-free aerobic oxidation of benzene to phenol, Sci. Rep 4 (2014) 3651–3655, https://doi.org/10.1038/srep03651.
[36] Z. Long, Y. Liu, P. Zhao, Q. Wang, Y. Zhou, J. Wang, Aerobic oxidation of benzene to phenol over polyoxometalate-paired PdII-coordinated hybrid: reductant-free heterogeneous catalysis, Catal. Commun. 59 (2015) 1–4, https://doi.org/10.1016/j.catcom.2014.09.031.
[37] Y. Morimoto, S. Bunno, N. Fujieda, H. Sugimoto, S. Itoh, Direct hydroxylation of benzene to phenol using hydrogen peroxide catalyzed by nickel complexes supported by pyridylalkylamine ligands, J. Am. Chem. Soc. 137 (2015) 5867–5870, https://doi.org/10.1021/jacs.5b01814.
[38] L. Losada-Garsia, A. Rodríguez-Otero, J. Palomo, Tailorable synthesis of heterogeneous enzyme–copper nanobiohybrids and their application in the

selective oxidation of benzene to phenol, Catal. Sci. Technol. 10 (2020) 196–200, https://doi.org/10.1039/C9CY02091H.
[39] Zh. Long, Y. Zhang, G. Chen, J. Shang, Y. Zhou, J. Wang, L. Sun, Nitrogen-doped biomass carbons meet with polyoxometalates: synergistic catalytic reductant-free aerobic hydroxylation of benzene to phenol, ACS Sustain. Chem. Eng. 7 (2019) 4230–4238, https://doi.org/10.1021/acssuschemeng.8b05920.
[40] S. Farahmand, M. Ghiaci, J. Razavizadeh, Copper phthalocyanine as an efficient and reusable heterogeneous catalyst for direct hydroxylation of benzene to phenol under mild conditions, Inorg. Chim Acta 484 (2019) 174–179, https://doi.org/10.1016/j.ica.2018.08.051.